OPTIMAL RANGES TO EVALUATE SUB-PIXEL CLASSIFCATIONS FOR LANDSCAPE METRICS

Amy E. Frazier*[1,2] and Le Wang[1,2]
*Corresponding Author
[1] University at Buffalo, Department of Geography, 105 Wilkeson Quad, Buffalo, NY 14261
[2] National Center for Geographic Information and Analysis, 301 Wilkeson Quad, Buffalo, NY 14261
Email: amy.frazier@gmail.com, lewang@buffalo.edu

ABSTRACT

Landscape metrics rely on classifications of remote sensing data, and errors inherent to the classification scheme will be propagated into any spatial pattern results. This issue is compounded for metrics derived from sub-pixel unmixing techniques, since a universal method for assessing the certainty of these soft classifications has not yet been accepted. This study investigates the role of sub-pixel classification accuracy on landscape metrics through a combination of mathematical, ecological, and remote sensing methods by evaluating the fragmentation of saltcedar, a weedy invasive plant species, in the Rio Grande basin. First, ecological curve fitting methods are adopted to model landscape metric response across sub-pixel land cover proportions, and the proportions affecting the greatest landscape structure changes are extracted. Second, the classification accuracy of the tessellated linear spectral unmixing technique (TLSU) is assessed at narrow fractional abundances to determine whether accuracy varies with land cover proportion. Lastly, the land cover proportions significantly influencing landscape structure are compared to the ranges of highest accuracy to examine how errors in the sub-pixel classification technique are propagated into metrics. Results show that curve fitting is an appropriate technique for modeling metric responses to sub-pixel land cover proportion, however optimal ranges differ depending on the particular metric. Classification accuracy varies across sub-pixel proportions, and pixels with lower fractional abundance exhibit higher mapping accuracies. Since the most accurate classification ranges are not always coincident with the optimal ranges for metric measurement, agreement should be tested before applying metrics to a research problem.

KEYWORDS: accuracy assessment, curve fitting, landscape metrics, optimal range, threshold, saltcedar, Landsat

INTRODUCTION

The fusion of remote sensing with landscape metrics to analyze spatial land cover patterns is the subject of countless remote sensing studies and is considered a leading research topic in landscape ecology (Peng et al., 2007). When used in tandem, the two methods couple the benefits of global spatial data coverage with the quantitative power of spatial statistics to produce a robust tool for characterizing spatial patterns. However, metric analyses typically rely on remote sensing classifications, and these classifications are subject to a host of errors and uncertainty (Shao & Wu, 2008). If not treated properly, these errors can be propagated into the spatial pattern analysis and will lead to inaccurate results.

Addressing the influence of classification accuracy on landscape metrics is an important research priority for both remote sensing (Liu & Chun, 2009; Zhang & Foody, 2009) and landscape ecology (Wu & Hobbs, 2002; Iverson, 2007), yet few studies have been conducted on this topic. Notably, Peng et al. (2007) analyze the influence of changing land use categorizations on a range of landscape metrics, and Shao and Wu (2008) discuss how classification accuracy can affect pattern analysis. These studies focus on pixel-based classifications though, and do not address the accuracy of metrics derived from sub-pixel data, which is an emerging focus area. When working with soft classifications, the complexity of dealing with multiple land covers for each pixel is magnified by the uncertainty of unmixing accuracy. Several techniques have been proposed to determine the accuracy of sub-pixel classifications (Binaghi et al., 1999; Gopal & Woodcock, 1994; Green & Congalton, 2004; Pontius & Cheuk, 2006; Silván-Cárdenas & Wang, 2008), but none have yet been adopted as a standard accuracy reporting measure.

This study aims to evaluate the effect of sub-pixel classification accuracy on landscape metrics by combining methods from remote sensing, ecology, and mathematics in an attempt to approach the problem from a new perspective. When landscape metrics are computed for sub-pixel classifications, the outcomes vary as a function of land cover proportion (Frazier & Wang, under review; Walsh et al., 2008), and response curves emerge when

sampled metric values are plotted against sub-pixel fractional abundances. These curves form as metrics respond to the environmental gradient of land cover proportion, and consequentially they closely resemble types of ecological curves formed by species responses to environmental gradients (see Austin et al., 1994; Bongers et al., 1999; Heikkinen & Mäkipää, 2010; Oksanen & Minchin, 2002). Also, much like ecological curves, metric curves are shaped by the underlying ecosystem processes driving the response. In this study, we apply curve fitting methods regularly employed in ecology to mathematically model and analyze metric responses in order to isolate the land cover proportions provoking the most significant changes in spatial pattern. These specific fractional abundance ranges are then utilized to guide a precise accuracy assessment to determine the effect of sub-pixel classification accuracy on metrics. To our knowledge, there are no known studies that apply curve fitting techniques to landscape metrics and use information derived from the curves to drive an analysis of error propagation.

The objectives of this study are to first standardize and interpret the shape and distribution of various metric response curves in order to extract the land cover proportions driving the most significant land cover changes. Second, the accuracy of the sub-pixel classification technique is evaluated at precise fractional abundance increments to determine whether classification accuracy varies with land cover proportion and to ascertain which proportions exhibit the highest accuracies. Lastly, by comparing the isolated ranges from the metric response curves with the most accurate fractional abundance ranges, the research tests which metrics integrate the highest classification accuracies and can therefore be reported most confidently.

BACKGROUND AND DATA

Invasive Species Detection and Mapping

Saltcedar (*Tamarix* spp.) is non-native, shrub-like vegetation that was originally introduced to the United States from Asia in the mid 19th century to provide windbreaks and erosion control along riverbanks. Since being introduced, it has invaded riparian sites throughout the southwestern U.S. and Mexico (Everitt et al., 1996) and has caused acute problems along the Rio Grande where its presence increases water shortages, raises soil and water salinity, and degrades wildlife habitats (Barz et al., 2009). High costs associated with eradication have spawned extensive research into remote sensing techniques for distinguishing saltcedar from native vegetation (Everitt & DeLoach, 1990; Everitt et al., 1996; Groeneveld & Watson, 2008; Hamada et al., 2007; Narumalani et al., 2009; Pu et al., 2008; Silván-Cárdenas & Wang, 2010) in order to map its spread. Sub-pixel classification techniques, in which each pixel is spectrally unmixed into multiple land covers, are a viable and accurate method to obtain detailed saltcedar land cover information when high resolution imagery is not available, and the tessellated linear spectral unmixing technique (TLSU) has been found to be superior to other linear and non-linear unmixing techniques for mapping saltcedar (Silván-Cárdenas & Wang, 2010). Utilizing the benefits of sub-pixel classifications, landscape metrics have been calculated to quantify the spatial and temporal distribution patterns of this highly invasive species (Frazier & Wang, under review).

Study Area

The study area is located along a 100 km stretch of the Rio Grande in southwest Texas referred to as the Forgotten River Reach. The area of investigation comprises the riparian buffer on both the U.S. and Mexico sides of the river (Fig. 1). This vegetated zone contains mostly saltcedar, but also includes mixes of native willow (*Salix* spp.) and mesquite (*Prosopis* spp.). The climate in the region is semi-arid to arid, with average annual rainfall amounts of less than 30 cm and maximum summer temperatures as high as 40^{o}C. Topography is characterized by canyons and small valleys with elevation ranging from 2500 m to 3000 m. In general, water sources in the region are scarce, and the presence of saltcedar exacerbates shortages.

Data Preprocessing

Nineteen Landsat images (path 31, row 39) collected between 1982 and 2009 comprise the remote sensing data for the study. Since the late-fall, early-winter period is the optimal time to distinguish saltcedar from native riparian vegetation (Everitt & DeLoach, 1990; Everitt et al., 1996), only images collected in late November through December were considered. The short temporal collection window precludes acquisition of a cloud-free image every year, and a total of 19 satisfactory images were selected from the 28-year time span. In the event that multiple cloud-free images were available in a single year, the image collected nearest to December 23rd was chosen, as this is the acquisition day of an Airborne Imaging Spectroradiometer for Applications (AISA) image used for radiometric correction and classification. Inclusion of a diverse set of images across a large collection period

is essential to accommodate multiple landscape structure stages, incorporate various extents of saltcedar invasion, and produce results that are applicable across the spatial and temporal extent of the ecosystem.

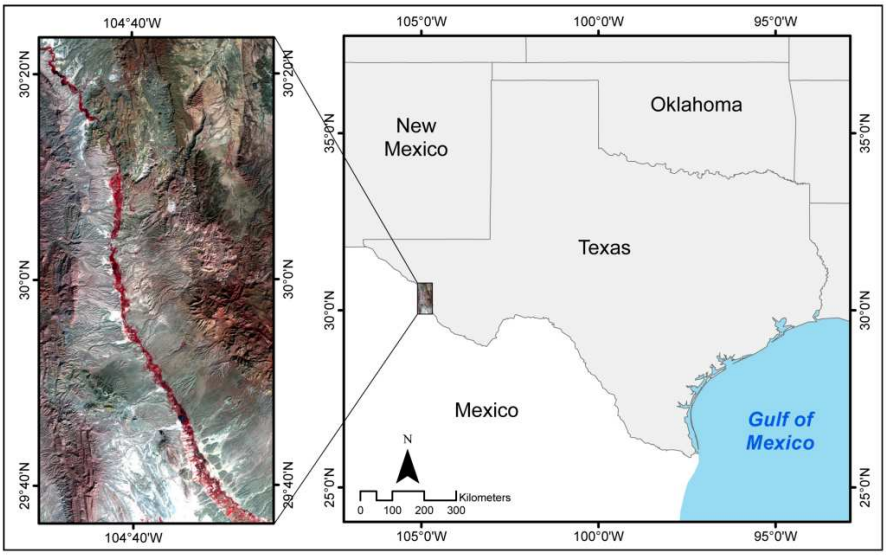

Figure 1. Location of cropped Landsat imagery along the Forgotten River Reach of the Rio Grande. Red false color composite highlights the vegetated riparian buffer strip, which is the area of investigation.

Images were corrected for atmospheric effects using the Iteratively Re-Weighted Multivariate Alternation Detection (IR-MAD) technique (Canty & Nielsen, 2008) with the AISA image acquired on December 23, 2005 serving as reference data. AISA was calibrated to measure 61 bands in the range of 430 to 1000 nm at a spatial resolution of 1 m. Bands 1 through 4 were extracted from each Landsat image to correspond with the spectral range of AISA for classification agreement.

METHODS

The methodology consists of three steps: (1) determine optimal sub-pixel proportions for measuring landscape structure changes using curve fitting techniques, (2) assess the accuracy of soft remote sensing classifications at specific proportional ranges to determine if accuracy varies with land cover proportions, and (3) compare the optimal ranges from the first step with the ranges of highest accuracy from the second step to determine how sub-pixel classification accuracy affects landscape metrics.

To derive optimal sub-pixel proportions, the data are linearly unmixed and the proportion of saltcedar is extracted from the classified raster. The data are then reclassified at multiple threshold cutoffs based on saltcedar abundance. Landscape metrics are computed for each threshold, and the results are plotted against fractional abundance threshold to produce metric response curves. These metric response curves are fit with mathematical models to enable sophisticated analysis, specifically identification of the land cover proportions causing the greatest metric changes. These abundances represent the optimal sub-pixel proportions for landscape pattern analysis.

The second part of the methodology involves a fine-scale accuracy assessment of the soft classifications at specific fractional abundance proportions using the root mean square error (RMSE) statistic. Finally, the proportions of highest accuracy are related to the optimal metric ranges to determine the effect of classification accuracy on spatial pattern results. The following sections describe these methods in detail.

Soft Classification

The 19 Landsat images are classified using TLSU (Silván-Cárdenas & Wang, 2010). TLSU is a soft classification technique which uses the concept of Delaunay tessellations to linearly unmix pixels (see Silván-Cárdenas & Wang, 2010). Calculations were completed in Matlab technical computing environment (The

Mathworks, Inc. 2002) and utilize hyperspectral measurements obtained from the AISA imagery. Endmembers were determined by averaging AISA reflectance values within ground truth GPS polygons for vegetated areas collected during field campaigns in 2004 and 2005. Additional polygons for non-vegetated endmembers were selected directly from on-screen visual interpretation. Pixels are unmixed into three classes: saltcedar, native vegetation, and other (Table 1). Proportions for each class are positive and must sum to one for each pixel.

Table 1. Classes and Associated Endmembers

Class	Endmember	Description
Saltcedar	Green saltcedar	*Tamarix* w/ green/brown foliage
	Senescent saltcedar	*Tamarix* w/ orange foliage
	Dry saltcedar	*Tamarix* w/ pale leaves
Native Vegetation	Gooding willow	*Salix goodingi*
	Mesquite	*Prosopis* spp.
	Poverty weed	*Iva* spp.
	Riparian bushes	Woody riparian species
Other	Creosote bush	Bush found among hillside
	Grasses	Dormant grass and weeds
	Herbaceous	Green herbaceous plants
	Gravel	Gravel road and desert gravel
	Soil	Bare ground, including sand
	Water	Rivers, ponds, lakes
	Wetlands	Emergent herbaceous wetlands
	Road	Paved road
	Roof	Multiple house roof types
	Shadow	Shadow on bare ground

Saltcedar proportions are extracted from each pixel for landscape metric analysis. An example of the saltcedar classification results for a portion of the study area is shown in Fig. 2. Red pixels contain high saltcedar proportions while green pixels contain low proportions. Saltcedar is most densely concentrated in the central areas of the riparian zone along the river.

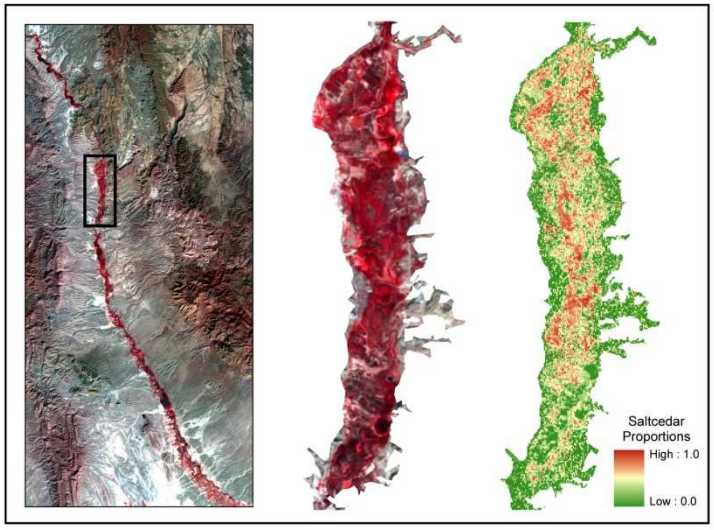

Figure 2. TLSU classification results. Left: entire study area showing location of zoomed in section for detail. Middle: color infrared Landsat image of the section of the area of investigation. Right: TLSU classification of the section showing the proportion of saltcedar for each pixel.

Data Discretization

Prior to computing landscape metrics, soft classified data must be discretized since metrics require bounded classes and cannot be computed directly from continuous sub-pixel data. Saltcedar fractions are hardened into bounded classes using the threshold continuum approach (Frazier & Wang, under review). In brief, this method reclassifies pixels based on presence-absence of saltcedar at specific fractional cover thresholds. Pixels with saltcedar proportions above the threshold are reclassified as 1 and included in metric analysis. Pixels that do not satisfy the threshold criteria are reclassified as 0 and excluded from analysis. The 19 classifications are subject to this reclassification process in 0.05 proportional increments from 0.0 to 1.0, which produces 21 separate presence-absence rasters for each year of imagery.

Landscape Metrics

Four metrics characterizing landscape fragmentation [Number of Patches (NP), Edge Density (ED), Patch Size Coefficient of Variation (PSCOV), and Largest Patch Index (LPI)] are calculated for each of the 21 presence-absence rasters for all 19 years. Metric values are plotted against fractional abundance thresholds, and data points are linearly interpolated to generate metric response curves (Fig. 3). Despite some variation, there are obvious trends across the fractional abundance thresholds for each metric.

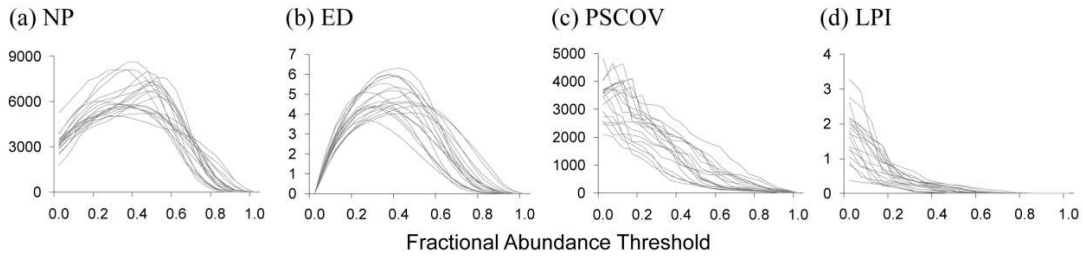

Figure 3. Metric response curves for (a) Number of Patches (NP), (b) Edge Density (ED), (c) Patch Size Coefficient of Variation (PSCOV), and (d) Largest Patch Index (LPI). Each graph contains 19 curves, one for each year of data.

Curve Fitting and Evaluation

Although measurement of metrics at specific fractional abundance thresholds is discrete, continuous trends emerge when sampled data are linearly interpolated, as shown in Fig. 3. Linear interpolation 'connects the dots' between measurements and can foster visual analysis of change. However, in any sampling program there is typically inherent random error associated with measurements, and basic linear interpolation will retain this error. Furthermore, sophisticated analyses cannot be performed on linear interpolations since they are not modeled mathematically. Curve fitting is the process of constructing a mathematical function that has the best fit for a set of data points. Fitting mathematical curves to raw data addresses the issue of random sampling error, supports interpolation of unmeasured values, and allows for interpretation of the data.

Theoretical Basis for Curve Fitting. The practice of fitting curves to environmental data arose from recognition that most physical phenomena are continual, but measurement of them is typically discrete (Lancaster and Salkauskas, 1986). Curve fitting has been widely adopted in the biological and ecological sciences in order to derive meaningful information from sampled environmental data (Bongers et al., 1999; Ficetola & Denoël, 2009; Heikkinen & Mäkipää, 2010), and with the rising costs associated with field surveying, the prediction of vegetation and other environmental values from environmental data is increasingly necessary. However, in depth analyses of these predicted data are only reliable once the basic shape of the response has been established (Austin et al., 1994).

Landscape metrics derived from soft classified remote sensing data are an ideal case for curve fitting since the ultimate goal of most spatial pattern studies is to uncover the underlying environmental and ecological processes driving landscape structure responses. Extant research in remote sensing is mainly limited to the use of curve fitting to determine the behavior of vegetation indices and to statistically fill or smooth data gaps for time periods where images are not available (Bradley et al., 2007; Carrao et al., 2010; Fang et al., 2008; Garung et al., 2009; Hermance et al., 2007; Jönsson et al., 2010). This research is the first known study to apply curve fitting procedures to landscape metrics, and explicitly to those derived from sub-pixel remote sensing classifications.

Cubic Polynomial Models. Among the various types of curves available to model environmental data, cubic polynomials are particularly well suited because they yield modal data, which have meaningful ecological

interpretation (Heikkinen & Mäkipää, 2010). Cubic polynomials are also advantageous because they capture the inflection point, the specific location where the curvature changes sign and reverses shape from concave up to concave down (or vice versa). The inflection point corresponds to the ecological threshold value where a break in slope occurs, and it signals an abrupt change in the ecosystem (Toms & Lesperance, 2003). Ascertaining the inflection point from fitted curves to determine significant points of change is used extensively in remote sensing to delimit the red-edge of spectral reflectance curves (Darvishzadeh et al., 2009; Gupta et al., 2003; Jayaraman & Srivastava, 2002; Ren et al., 2010), however to our knowledge this research is the only study applying these mathematical and ecological interpretation techniques to landscape metrics.

Based on the fundamental shape of the NP and ED response curves (see Fig. 3), these two metrics are best modeled with cubic polynomials. The curve fitting procedure calculates the cubic polynomial equation that will most closely fit the measured data points and fits that equation line to the data. The equation can then be used to derive complex ecological information from the curve. Metric response curves are each fit with a separate cubic polynomial equation producing 19 mathematical curves for each metric (Fig. 4). All curve fitting was completed using the Curve Fitting Toolbox in the Matlab computing environment (The Mathworks Inc., 2002).

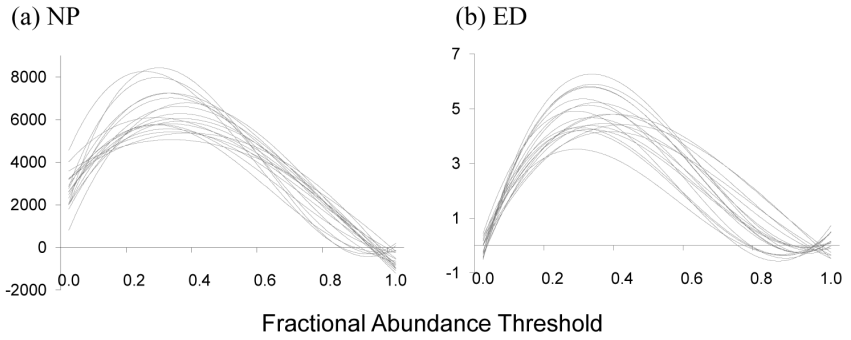

Figure 4. Cubic polynomial curves fit to the 19 years of measured metric data for (a) Number of Patches (NP) and (b) Edge Density (ED).

Exponential Decay Models. The basic shape of the PSCOV and LPI response curves do not follow the typical trends of cubic polynomials (see Fig. 3) and therefore must be fit with a different type of model. After testing the fit of various curves, exponential decay curves, which have been used in ecology to model community structure as a function of habitat size (Millar et al., 2005), were selected. Exponential decay curves decrease at a rate which is proportional to the value of x, where x in this case is the fractional abundance threshold. The greatest rate of change occurs at the lowest values of x, and each increasing step in threshold exhibits progressively smaller amounts of change until an asymptote is eventually approached. The modeled exponential decay response curves for PSCOV and LPI are shown in Fig. 5.

Ecological Interpretation of Optimal Ranges. Curve interpretation for ecosystem studies utilizes ecological thresholds, the points or zones of abrupt change in an ecosystem property where small changes in an environmental driver produce a large ecosystem response (Ficetola & Denoël, 2009; Groffman et al., 2006; Muradian, 2001). Ecological thresholds are significant to ecosystem management because they signal the point along the environmental gradient where the dependent variable is most sensitive, and they can be located on curves through mathematical derivatives. The derivative of a point on the curve equals the slope of the tangent line to the graph of the function at that point. By calculating the first derivative of the curve, the fractional abundance value for the local minimum and maximum metric values can be determined. Likewise, the second derivative will produce a value for the inflection point. This inflection point is the location where the greatest change in metric takes place across the smallest change in fractional abundance threshold.

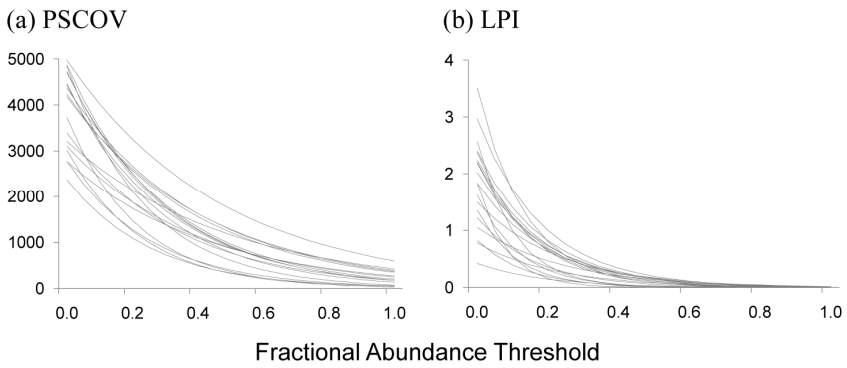

Figure 5. Exponential decay curves fit to the 19 years of measured metric data for (a) Patch Size Coefficient of Variation (PSCOV) and (b) Largest Patch Index (LPI).

First and second derivatives are calculated for all NP and ED curves, and the fractional abundance threshold values for the 19 inflection points are averaged for each metric. Ecological studies typically employ a one standard deviation envelope around the mean to determine species abundance envelopes (Birks et al., 1990; Huff et al., 2005). Therefore, a one standard deviation envelope was constructed around the mean inflection point to delineate the optimal range of land cover proportions from which to calculate each respective landscape metric.

Exponential decay curves do not inflect, and therefore optimal ranges must be evaluated using different criteria. The greatest rate of change in an exponential decay curve occurs at the smallest fractional abundance threshold. In order to standardize the ranges across the two types of curves, the average metric change absorbed by the envelope for the polynomial curves (45%) is applied to the exponential decay curves to determine the extent of the range envelopes. The envelopes for PSCOV and LPI originate at 0.0 and increase until 45% of the values along the average curve are included. This method to standardize multiple curves using the percentage of values encompassed by the envelope is applicable for comparison of many types of curves, not just those utilized in this study.

Accuracy Assessment

The second step of the methodology is to assess the accuracy of the sub-pixel classification technique. TLSU accuracy is assessed using RMSE. RMSE expresses the magnitude of the average error generated by the classification and is commonly used to validate spectral unmixing results (Foody et al., 2010; Mishra et al., 2009; Pacheco & McNairn, 2010), although it is not known to have ever been used to test sub-pixel classification accuracy in landscape metric applications. A spectral angle mapper (SAM) classification generated from the AISA image serves as the basis for the reference data. SAM assigns a single class (see Table 1) to each 1m AISA pixel using ground truth reflectances collected during the 2004 and 2005 field campaigns. The SAM classification is aggregated to 30m (hereafter referred to as $AISA_{30}$) to match the spatial resolution of the Landsat data, and reference saltcedar proportions are calculated for each $AISA_{30}$ pixel. There is no cloud-free Landsat TM image available from 2005 to correspond with the acquisition date of the AISA image. Therefore, the 2004 image is used. Based on knowledge gained from the 2004 and 2005 field campaigns, care has been taken to assure that no significant landscape changes occurred within the study area during this time period.

To select pixels for the accuracy assessment, ten 10x10 grids (1,000 pixels) are randomly placed in the region covered by the AISA image, and corresponding pixels from the $AISA_{30}$ and the 2004 TLSU classification are extracted. The 1,000 test pixels are divided into ten distinct ranges based on the $AISA_{30}$ sub-pixel proportions (i.e., 0.0-0.1, 0.1-0.2, etc.), and are referred to hereafter as proportional ranges (PR). RMSE values are calculated for each PR using the following equation:

$$\mathrm{RMSEPR} = \sqrt{\frac{\sum_{i=1}^{n}(Ri - Ai)^2}{n-1}}$$

where R_i is the proportion of saltcedar in the reference pixel ($AISA_{30}$), A_i is the proportion of saltcedar in the assessed pixel (2004 TLSU), and n is the number of reference pixels in each range. In step three of the methodology, RMSE accuracies are compared to landscape metrics to determine whether the highest classification accuracies coincide with the optimal ranges at which to measure metrics.

RESULTS AND DISCUSSION

Curve Fitting

According to coefficient of determination (R^2) values (Table 2), fitted curves correlate very highly with actual measured metric values. The majority of R^2 values are above 0.9, and all values are above 0.84, which is an excellent fit for all curves. The strong predictive capability of the models is due to proper curve selection for each metric based on the trends that emerged from linear interpolation of the initial metric response data. These high performance values support the assumption that landscape structure is ultimately driven by natural ecosystem processes related to land cover proportions.

Table 2: R^2 Values for Fitted Curves

Image	R^2 Values			
Year	NP*	ED*	PSCOV†	LPI†
1982	0.9955	0.9803	0.8887	0.9684
1984	0.9860	0.9718	0.9608	0.9516
1985	0.9536	0.9985	0.9589	0.9845
1986	0.9655	0.9826	0.9826	0.9742
1992	0.8648	0.9675	0.9417	0.9771
1993	0.9304	0.9869	0.9005	0.9708
1994	0.9825	0.9616	0.9104	0.9793
1995	0.9565	0.9986	0.9799	0.9874
1996	0.8852	0.9833	0.9032	0.9837
1997	0.9867	0.9773	0.9396	0.9673
1998	0.9472	0.9665	0.8439	0.9870
1999	0.9163	0.9785	0.9077	0.9525
2000	0.9617	0.9850	0.9691	0.9812
2002	0.9237	0.9829	0.9064	0.9614
2003	0.8843	0.9754	0.9703	0.9937
2004	0.9528	0.9709	0.9893	0.9870
2006	0.8672	0.9784	0.9392	0.9500
2008	0.9899	0.9973	0.9158	0.9389
2009	0.9372	0.9915	0.9223	0.9742

*Data modeled using cubic polynomial curves
†Data modeled using exponential decay curves

Optimal Threshold Ranges

Optimal ranges for testing the four metrics are given in Table 3. The metrics fit with cubic polynomials (NP and ED) have average inflection points of 0.73 and 0.65 respectively. Therefore the optimal ranges encompass higher saltcedar proportions than PSCOV and LPI, since the ranges for those two metrics begin at zero. There are slight differences in range size between metrics, with a maximum of 0.22 for NP and a minimum of 0.10 for PSCOV. However, since the ranges were selected to include equivalent amounts of data values, these small variations are inconsequential.

Table 3. Average Inflection Points and Optimal Fractional Abundance Ranges for Metric Measurement

Metric	Average Inflection Point	Standard Deviation	Optimal Range
Number of Patches (NP)	0.73	0.11	0.62 - 0.84
Edge Density (ED)	0.65	0.10	0.55 - 0.75
Patch Size Coefficient of Variation (PSCOV)	-	-	0.00 - 0.10
Largest Patch Index (LPI)	-	-	0.00 - 0.21

Proportional Range Error

Classification accuracy was evaluated using RMSE, and results are given in Table 4. Low RMSE values indicate better accuracy. The classification performed best in PR 0.2-0.3 with an RMSE of 0.192, followed by PR 0.1-0.2 and 0.3-0.4 with RMSE values of 0.206 and 0.214 respectively. Overall, TLSU was more accurate for lower sub-pixel ranges, with the five lowest RMSE values occurring in the lowest five PRs. Highest RMSE, indicating low classification accuracy, are found in PR 0.8-0.9 and 0.9-1.0 with 0.580 and 0.579 respectively.

Table 4. Root Mean Square Error (RMSE) Results for Sub-Pixel Proportional Ranges

Proportional Range (PR)	Reference Pixels (n)	RMSE
0.0-0.1	238	0.280
0.1-0.2	90	0.206
0.2-0.3	110	0.192
0.3-0.4	85	0.214
0.4-0.5	94	0.236
0.5-0.6	85	0.320
0.6-0.7	86	0.359
0.7-0.8	55	0.450
0.8-0.9	66	0.580
0.9-1.0	91	0.579

One possible explanation for the pattern of high accuracies in low saltcedar proportions is the distinctive spectral characteristics of endmembers for the non-vegetated other class (see Table 1) versus those for the vegetated saltcedar and native vegetation classes. The distinct endmembers may achieve accurate mapping of pixels with high proportions of non-vegetated areas (and consequently low proportions of saltcedar or other vegetation). Spectral signatures for saltcedar and native vegetation are more closely related. Coupled with having all vegetation clustered within the narrow riparian zone, the classification may not produce accurate results when saltcedar and native vegetation are mixed together in high proportions, and this may have resulted in lower classification accuracies. Further research investigating the exact breakdown of land cover proportions for pixels classified incorrectly is necessary to determine if specific classes influence the classification accuracy. Overall, the accuracy results are encouraging as there is evidence to suggest that detection and control of invasive species is most crucial early on in the invasion process (Hamada et al., 2007; Walsh et al., 2008). With high accuracy at low proportions, saltcedar is best detected in the early stages of its spread.

Metric Performance

To assess the effect of sub-pixel classification accuracy on landscape metrics, RMSE PR values are interpolated to the optimal metric ranges (see Table 3). For metrics with optimal ranges stretching across multiple RMSE ranges, a weighted sum is calculated by multiplying the percent of the range within the PR by the RMSE summing across the range. In this way, RMSE for the ranges can be compared. Results (Table 5) show that LPI has the lowest aggregated RMSE for its optimal sampling range at 0.240, followed by PSCOV with 0.280. NP has the highest aggregated RMSE and therefore encompasses the lowest classification accuracy.

Table 5. Root Mean Square Error (RMSE) Values for Metric Optimal Ranges

Metric	Optimal Range RMSE
Number of Patches (NP)	0.441
Edge Density (ED)	0.305
Patch Size Coefficient of Variation (PSCOV)	0.280
Largest Patch Index (LPI)	0.240

Overall, these results indicate that there are differences in the accuracy of the soft classification at different PRs, and these varying accuracies can affect metric measurements. In general, the RMSE values in Table 5 are highly dependent on the alignment of the highest accuracies with the optimal range for measurement. The superior performance of TLSU at lower fractional abundance ranges combined with the high initial rates of change for the exponential decay models explain the higher accuracies of PSCOV and LPI compared to NP and ED. These results do not aim to denigrate the usefulness of specific landscape metrics nor do they attempt to promote the use of certain metrics over others. Rather, these results highlight that classification accuracy does not affect all metrics evenly, and certain metrics may be more robust to measure spatial patterns in a certain study given the accuracy of a specific classification scheme.

CONCLUSIONS

Measures that rely on remote sensing classifications are subject to error propagation from those classifications, yet little research has been conducted to deduce the impact of classification accuracy on spatial patterns. Building on previous research, which found that landscape metrics vary as a function of land cover proportion, this study tested the application of ecological curve fitting techniques to remote sensing-derived spatial patterns, interpreted those curves in the context of the sub-pixel proportions driving metric changes, and assessed the accuracy of a sub-pixel classification technique in relation to the landscape metrics derived from it.

Several key findings emerge from this research. First, this study found that ecological curve fitting methods are appropriate and practical for mathematically analyzing landscape metric data derived from sub-pixel remote sensing classifications. Metric responses to varying land cover proportions behave similarly to species responses across ecological gradients, and it is probable that landscape structure changes are driven by underlying ecosystem processes. Determining saltcedar proportions that induce the most extreme shifts in structural response is the first step to eventually controlling invasion. These proportions can also be used by ecosystem managers to target areas for eradication and control measures.

A second key finding from this work is that the classification accuracy of the TLSU technique is not constant across all fractional abundances. Accuracies are higher for pixels with low saltcedar proportions. These higher accuracies may stem from the distinct spectral signatures of the non-vegetated class which aid in mapping pixels with minimal amounts of saltcedar or native vegetation. However, this finding is unexpected since pure spectral endmembers were collected for all classes within the area of investigation. The pure pixels representing the reflectance values for 100 percent saltcedar land cover proportion should have generated high accuracy when mapping other pixels dominated by high proportions of saltcedar.

Finally, comparison between the ranges with highest sub-pixel classification accuracy and the selected ranges for metric measurement determined that these two sets of optimal ranges do not always coincide. Optimal metric performance depends on proper alignment of the most accurate classification ranges. Since each metric is optimally measured at different fractional abundance thresholds, accuracy should be tested and compared before applying metrics to sub-pixel data.

Developing landscape metrics from sub-pixel, or soft classifications is a relatively new research focus, but one that deserves attention considering recent advances in spectral unmixing techniques. Future work should investigate error propagation from the perspective of both the magnitude of classification errors across land cover proportions as well as the spatial variability of classification errors. Examining the distribution of varying degrees of accuracy across the landscape may provide insight into the spatial processes affecting saltcedar invasion.

REFERENCES

Austin, M.P., A.O. Nicholls, M.D. Doherty, and J.A. Meyers, 1994. Species Response Functions to an Environmental Gradient by Means of a β-Function. *J Veg Sci*, 5(2): 215-228.

Barz, D., R. Watson, J. Kanney, J. Roberts, and D. Groeneveld, 2009. Cost/Benefit Considerations for Recent Saltcedar Control, Middle Pecos River, New Mexico. *Environ Manage*, 43: 282-298.

Bekker, M., J. Clark, and M. Jackson, 2009. Landscape metrics indicate differences in patterns and dominant controls of ribbon forests in the Rocky Mountains, USA. *Appl Veg Sci*, 12(2): 237-249.

Binaghi, E., P.A. Brivio, P. Chezzi, and A. Rampini, 1999. A fuzzy set-based assessment of soft classification. *Pattern Recognition Letters*, 20:935-948.

Birks, H., J. Line, S. Juggins, A. Stevenson, and C. ter Braak, 1990. Diatoms and pH reconstruction. *Philosophical Transactions of the Royal Society of London B*, 327: 263-278.

Bongers, F., L. Poorter, R. Van Rompaey, and M. Parren, 1999. Distribution of twelve moist forest canopy tree species in Liberia and Côte d'Ivoire: response curves to a climatic gradient. *J Veg Sci*, 10: 371-382.

Bradley, B.A., R.W. Jacob, J.F. Hermance, and J.F. Mustard, 2007. A curve fitting procedure to derive inter-annual phonologies from time series of noisy satellite NDVI data. *Remote Sens Environ*, 106(2): 137-145.

Brown, D., J. Duh, and S. Drzyzga, 2000. Estimating error in an analysis of forest fragmentation change using North American Landscape Characterization (NALC) data. *Remote Sens Environ*, 71(1): 106-117.

Canty, M. J, and A.A. Nielsen, 2008. Automatic radiometric normalization of multitemporal satellite imagery with the iteratively re-weighted MAD transformation. *Remote Sens Environ*, 112(3): 1025-1036.

Carrao, H., P. Goncalves, and M. Caetano, 2010. A Nonlinear Harmonic Model for Fitting Satellite Image Time Series: Analysis and Prediction of Land Cover Dynamics. *IEEE T Geosci Remote*, 48(4): 1919-1930.

Darvishzadeh, R., C. Atzberger, A.K. Skidmore, and A.A. Abkar, 2009. Leaf Area Index derivatrion from hyperspectral vegetation indicies and the red edge position. *Int J Remote Sens*, 30(23): 6199-6218.

Everitt, J. H., and C.J. Deloach, 1990. Remote-Sensing Of Chinese Tamarisk (Tamarix-Chinensis) and Associated Vegetation. *Weed Sci*, 38(3): 273-278.

Everitt, J. H., D.E. Escobar, M.A. Alaniz, M.R. Davis, and J.V. Richerson, 1996. Using spatial information technologies to map Chinese tamarisk (Tamarix chinensis) infestations. *Weed Sci*, 44(1): 194-201.

Fang, H.L., S.L. Liang, J.R. Townshend, and R.E. Dickinson, 2008. Spatially and temporally continuous LAI data sets based on an integrated filtering method: Examples from North America. *Remote Sens Environ*, 112(1): 75-93.

Ficetola, G., and M. Denoël, 2009. Ecological thresholds: an assessment of methods to identify abrupt changes in species-habitat relationships. *Ecography*, 32: 1075-1084.

Foody, G., R. Lucas, P. Curran and M. Honzak, 2010. Non-linear mixture modeling without end-members using an artificial neural network. *Int J Remote Sens*, 18(4): 937-953.

Frazier, A.E. and L. Wang. Evaluation of soft classifications for characterizing spatial patterns of invasive species. *Remote Sens Environ*, (under review).

Garung, R., F. Breidt, A. Dutin, and S. Ogle, 2009. Predicting Enhanced Vegetation Index (EVI) curves for ecosystem modeling applications. *Remote Sens Environ*, 113: 2186-2193.

Gopal, S., and C.E. Woodcock, 1994. Theory and methods for accuracy assessment of thematic maps using fuzzy sets. *Photogramm Eng Rem S*, 60(2): 181−188.

Green, K., and G. Congalton, 2004. An error matrix approach to fuzzy accuracy assessment: The NIMA geocover project. In R. S. Lunetta & J.G. Lyon (Eds.), Remote sensing and GIS accurcacy assessment (pp. 163−172). Boca Raton: CRC Press.

Groeneveld, D. P., and R.P. Watson, 2008. Near-infrared discrimination of leafless saltcedar in wintertime Landsat TM. *Int J Remote Sens*, 29(12): 3577-3588.

Groffman, P., J. Baron, T. Blett, A. Gold, I. Goodman, L. Gunderson, B. Levinson, M. Palmer, H. Paerl, G. Peterson, N. Poff, D. Rejeski, J. Reynolds, M. Turner, K. Weathers, and J. Wiens, 2006. Ecological Thresholds: The Key to Successful Environmental Management or an Important Concept with No Practical Application? *Ecosystems*, 9: 1-13.

Gupta, R.K., D. Vijayan, T.S. Prasad, 2003. Comparative analysis of red-edge hyperspectral indices. *Adv Space Res*, 32(11): 2217-2222.

Hamada, Y., D.A. Stow, L.L. Coulter, J.C. Jafolla, and L.W. Hendricks, 2007. Detecting Tamarisk species (Tamarix spp.) in riparian habitats of Southern California using high spatial resolution hyperspectral imagery. *Remote Sens Environ*, 109(2): 237-248.

Harold, M., H. Couclelis, and K. Clarke, 2005. The role of spatial metrics in the analysis and modeling of urban land use change. *Comput Environ Urban*, 29: 369-399.

Heikkinen, J., and R. Mäkipää, 2010. Testing hypotheses on shape and distribution of ecological response curves. *Ecol Model*, 221: 388-399.

Hermance, J., R. Jacob, B. Bradley, and J. Mustard, 2007. Extracting Phenological Signals from Multiyear AVHRR NDVI Time Series: Framework for Applying High-Order Annual Splines with Roughness Damping. *IEEE T Geosci Remote*, 45(10): 3264-3276.

Huff, D., S. Hubler, and A. Borisenko, 2005 Using Field Data to Estimate the Realized Thermal Niche of Aquatic Vertebrates. *N Am J Fish Manage*, 25: 346-360.

Iverson, L., 2007. Adequate data of known accuracy are critical to advancing the field of landscape ecology. In: Wu J, Hobbs R (eds) Key topics in landscape ecology. Cambridge University Press, Cambridge, UK, pp 11–38.

Jayaraman, V. and S.K. Srivastava, 2002. The invariance of red-edge inflection wavelengths derived from ground based spectro-radiometer and space-borne IRS-P3: MOS-B data. *Int J Remote Sens*, 23(14): 2741-2765.

Jönsson, A.M., L. Eklundh, M., Hellström, L. Bärring, and P. Jönsson, 2010. Annual changes in MODIS vegetation indices of Swedish coniferous forests in relation to snow dynamics and tree phenology. *Remote Sens Environ*, 114(11): 2719-2730.

Lancaster, P. and K. Salkauskas, 1986. Curve and Surface Fitting: An Introduction. Academic Press: New York.

Liu, D. and Y. Chun, 2009. The effects of different classification models on error propagation in land cover change detection. *Int J Remote Sens*, 30(20): 5354-5364.

Millar, R.B., M.J. Anderson, and G. Zunun, 2005. Fitting nonlinear environmental gradients to community data: A general distance-based approach. *Ecology*, 86(8): 2245-2251.

Misra, V.D., H.S. Negi, A.K. Rawat, A. Chaturvedi, and R.P. Singh, 2009. Retrieval of sub-pixel snow cover information in the Himalayan region using medium and coarse resolution remote sensing data. *Int J Remote Sens*, 30(18): 4707-4731.

Muradian, R., 2001. Ecological thresholds: a survey. *Ecological Economics*, 38: 7-24.

Narumalani, S., D.R. Mishra, R. Wilson, P. Reece, and A. Kohler, 2009. Detecting and Mapping Four Invasive Species along the Floodplain of North Platte River, Nebraska. *Weed Technol*, 23(1): 99-107.

Oksanen, J., and P.R. Minchin, 2002. Continuum theory revisited: what shape are species responses along ecological gradients. *Ecological Modelling*, 157: 119-129.

Pacheco, A. and H. McNairn, 2010. Evaluating multispectral remote sensing and spectral unmixing analysis for crop residue mapping. *Remote Sens Environ*, 114: 2219-2228.

Pontius, R. G., and M.L. Cheuk, 2006. A generalized cross-tabulation matrix to compare soft-classified maps at multiple resolutions. *Int J Geogr Inf Sci*, 20(1): 1-30.

Pu, R. L., P. Gong, Y. Tian, X. Miao, R.I. Carruthers, and G.L. Anderson, 2008. Using classification and NDVI differencing methods for monitoring sparse vegetation coverage: a case study of saltcedar in Nevada, USA. *Int J Remote Sens*, 29(14): 3987-4011.

Peng, J., Y. Wang, M. Ye, J. Wu, and Y. Zhang, 2007. Effects of land-use categorization on landscape metrics: A case study in urban landscape of Shenzhen, China. *Int J Remote Sens*, 28(10): 4877-4895.

Ren, H.Y., D.F. Zhuang, J.J. Pan, X.Z. Shi, R.H. Shi, and H.J. Wang, 2010. Study on Canopy Spectral Characteristics of Paddy Polluted by Heavy Metals. *Spectrosc Spect Anal*, 30(2): 430-434.

Shao, G. and J. Wu, 2008. On the accuracy of landscape pattern analysis using remote sensing data. *Landscape Ecol*, 23: 505-511.

Silván-Cárdenas, J. L. and L. Wang, 2008. Sub-pixel confusion-uncertainty matrix for assessing soft classifications. *Remote Sens Environ*, 112(3): 1081-1095.

Silván-Cárdenas, J. L., and L. Wang, 2010. Retrieval of subpixel Tamarix canopy cover from Landsat data along the Forgotten River using linear and nonlinear spectral mixture models. *Remote Sens Environ*, 114(8): 1777-1790.

Toms, J. and M. Lesperance, 2003. Piecewise Regression: A Tool for Identifying Ecological Thresholds. *Ecology*, 84(8): 2034-2041.

Walsh, S., A. McCleary, C. Mena, Y. Shao, J. Tuttle, and A. Gonzalez, 2008. QuickBird and Hyperion data analysis of an invasive plant species in the. Galapagos Islands of Ecuador: Implications for control and land use management. *Remote Sens Environ*, 112(5): 1927-1941.

Wu, J. and R. Hobbs, 2002. Key issues and research priorities in landscape ecology: An idiosyncratic synthesis. *Landscape Ecol*, 17: 355-365.

Zhang, J., and G. Foody, 2009. Preface: Spatial accuracy in remote sensing. *Int J Remote Sens*, 30(20): 5239-5242.